Dependence of Optical Diffusion Tomography Image Quality on Image Operator and Noise

Jenghwa Chang [1], Harry L. Graber [2], Randall L. Barbour [1,2]

SUNY Health Science Center at Brooklyn,
Dept. of Pathology [1], and Physiology and Biophysics [2]

ABSTRACT

By applying linear perturbation theory to the radiation transport equation, the inverse problem of optical diffusion tomography can be reduced to a set of linear equations, $\mathbf{W}\mu = \mathbf{R}$, where $\mathbf{W}$ is the weight function, μ is the cross section perturbations to be imaged, and $\mathbf{R}$ is the detector readings perturbations. The quality of reconstructed images depends on the accuracy of $\mathbf{W}$ and $\mathbf{R}$, and was studied by corrupting one or both with systematic error and/or random noise. Monte Carlo simulations (MCS) performed on a cylindrical phantom of 20 mean free paths (mfp) diameter, with and without a black absorber located off–axis, were used to compute $\mathbf{R}$ and $\mathbf{W}$ (*i.e.*, matched $\mathbf{W}$). Additional MCS computed $\mathbf{W}$s for cylinders of 10 mfp, 40 mfp, and 100 mfp diameters (*i.e.*, *un*matched $\mathbf{W}$). $\mathbf{R}$ and/or $\mathbf{W}$ also were corrupted with additive white noise. A constrained CGD method we developed was used to reconstruct images from the simulated $\mathbf{R}$ and $\mathbf{W}$s. The results show that images containing few artifacts and the rod accurately located can be obtained when the matched $\mathbf{W}$ is used. Comparable image quality was obtained for unmatched $\mathbf{W}$s, but the location of the rod becomes more inaccurate as the mismatch increases. The noise study shows that $\mathbf{W}$ is much more sensitive than $\mathbf{R}$ to noise. The rod can be reasonably located with 100% noise added to $\mathbf{R}$, while addition of 5% noise to $\mathbf{W}$ totally destroys the image. The impact of noise increases with the number of iterations.

I. INTRODUCTION

There has been sufficiently extensive development of optical diffusion tomography in recent years that some applications are ready for clinical testing [1]. Two types of tomographic schemes have been used. In cross section imaging, first proposed by our group and later also adopted by many other teams [2], one tries to map the perturbations of physical properties such as the scattering and absorption cross sections relative to a reference state, as a function of physiological or pathological conditions, *e.g.*, brain tumor or breast cancer. The newly developed luminescence imaging [3] uses a similar idea, by assuming that the presence of fluorophore/phosphor slightly perturbs the background absorption cross section and taking advantage of the difference between the excitation and emission spectra of the fluorescence or phosphorescence phenomena in order to image the fluorophore/phosphor concentration and mean lifetime as a function of physiological or pathological condition. In either case, the inverse problem reduces to a system of linear equations [3,4] of the form $\mathbf{W}\mu = \mathbf{R}$ when it is based on a perturbed transport equation. Here, $\mathbf{W}$ is the weight matrix, whose elements are proportional to products of forward (from source to voxel) and adjoint (from voxel to detector) intensities; μ is the quantity to be imaged; and $\mathbf{R}$ is the detector readings.

Because both imaging techniques employ perturbation methods, the quality of reconstructed images is a function of modeling error, that is, the accuracy of the weight matrix calculated based on the reference medium (cross section imaging) or on the background medium (luminescence imaging). We have studied two methods for estimating the physical properties of the reference or background medium in the (realistic) case in which they are not known *a priori*. In the first [5], one begins with a simple preselected medium, typically in a homogeneous state, and repeatedly alternates between solving the perturbation equation for μ and computing a new $\mathbf{W}$ based on the current estimate of μ. This is similar to the iterated Born approximation used in microwave imaging [6] and is generally very computation –intensive because multiple forward calculations are needed to update the weight matrix. The second method [7] assigns the average physical properties of the various tissue types known to be present in a given sample to an anatomically accurate map obtained from some other imaging modality, *e.g.*, CT, MRI. This requires image segmentation and registration techniques to process the anatomical images, but these are generally much faster than updating the forward calculation. In the best case, a single step of solving the forward and inverse problems would suffice. If it should still prove necessary in practice to repeat the process, the number of iterations required would be much smaller under this approach than by starting from an assumption of homogeneity. The probability of the iterative process diverging would likewise be much smaller.

Previous studies [8,9] also have shown that $\mathbf{W}$ is an ill–conditioned matrix; thus, the reconstructed result is very sensitive to noise. In general, two types of noise are encountered in an optical imaging system. The first one is Poisson noise due to the inherent statistical variations in the mechanisms of photon generation and interaction with the target medium, and can be reduced by increasing either the source intensity or the detector acquisition time. The second is independent additive noise that manifests as dark current in the counter and electronics, and also arises as a

0-7803-3180-X/96$5.00©1996

consequence of numeric errors. Its effect can be lessened by proper filtering.

Since the exact structure of the reference medium is not known in most cases, it is important to study the impact of modeling error and random noise on reconstructed images. In this study, systematic mismatches were introduced in the weight matrices by reconstructing images of a simple phantom using weight matrices from reference media with different physical properties. In addition, random Gaussian noise at different levels was added to the detector readings and/or weight matrices to examine its effect on the reconstructed images.

II. THEORY

The inverse problems for absorption cross section imaging or fluorescent imaging reduce to a system of linear equations,

$$\mathbf{W}\boldsymbol{\mu} = \mathbf{R}\,, \tag{1}$$

where $\mathbf{W}$ is the weight matrix, $\boldsymbol{\mu}$ is the vector of unknown absorption cross sections or products of fluorophore concentration and quantum yield, and $\mathbf{R}$ is the vector of detector readings. In absorption cross section imaging [4], Eq. (1) is a discretized version of an integral equation,

$$\Delta R = \int_V w_a \Delta\mu_a d^3r \tag{2}$$

where $\Delta\mu$ is the *macro*scopic absorption cross section perturbation [mm^{-1}], ΔR is the detector reading perturbation, and w_a is the *weight function*,

$$w_a = -\left(\phi_0\phi_0^+ - \mathbf{J}\cdot\mathbf{J}^+\right)\Big/4\pi\,, \tag{3}$$

where

$$\phi_0 = \int_{4\pi}\phi d\Omega\,, \qquad \mathbf{J} = \int_{4\pi}\phi\Omega d\Omega\,,$$

$$\phi_0^+ = \int_{4\pi}\phi^+ d\Omega\,, \qquad \mathbf{J}^+ = -\int_{4\pi}\phi^+\Omega d\Omega\,,$$

and ϕ and ϕ^+ are forward (from a source to a voxel) and adjoint (from a voxel to a detector) angular intensities, obtained by solving a transport equation [4]. In the fluorescence imaging case [3], Eq. (1) is a discretized version of

$$R = \int_V w_{fl}\left(\gamma N_0\right)d^3r\,, \tag{4}$$

where R is the emitted fluorescence intensity, γ is the quantum yield, N_0 is the fluorophore concentration, and

$$w_{fl} = \Sigma_{T,1\to 2}\phi_0^1\phi_0^{2^+}\Big/4\pi\,, \tag{5}$$

where $\Sigma_{T,1\to 2}$ is the *micro*scopic total cross section [mm^2] introduced by the fluorophore, and ϕ_0^1 and $\phi_0^{2^+}$ are, respectively, the forward and adjoint integrated intensities of the exciting and emitted light. Because $\mathbf{J}\cdot\mathbf{J}^+$ is generally much smaller than $\phi_0\phi_0^+$, w_a for the cross section imaging problem can be well approximated by including only the first term in the numerator of Eq. (3). In this sense, the weight matrix in both the cross section imaging and fluorescence imaging cases are essentially the same, and the findings of studies of one imaging modality will also apply for the other.

III. METHOD

Two sources of error were introduced in this study. The first is a systematic error, produced by varying the total cross section of the reference medium. Monte Carlo simulations (MCS) modeled light propagation in a cylindrical phantom of 20 mean free paths (mfp) diameter, as shown in Figure 1, with and without a black absorber at an off–axis location. The perturbed detector readings, $\mathbf{R}$, were obtained by calculating the differences, at all detector locations, between the detected intensities in the absence and presence of the black rod. The matched weight matrix $\mathbf{W}$ was calculated from the forward and adjoint collision densities in each voxel. The simulated $\mathbf{R}$ and $\mathbf{W}$ are essentially noiseless except for Poisson noise arising from the MCS, which is negligible since O(10^8) photons were simulated and correlated sampling was used for variance reduction. MCS were also performed to get unmatched weight matrices from media of 10 mfp, 40 mfp, and 100 mfp diameter. This is equivalent to varying the total cross section while keeping the physical dimensions of the phantom constant. The matched and unmatched matrices were also used for image reconstruction from experimental data. Figure 2A shows a sketch of the tissue phantom and Figure 2B shows face–on and edge–on views of the disk that anchors the absorbing rods at the bottom. An 8 cm (i.d.) cylinder was filled to a height of 35 cm with a suspension of Intralipid® fat emulsion diluted with water. Measurements were performed on suspensions containing 2% lipid by volume, which was prepared by performing a 1:5 dilution of the commercially available 10% stock solution. The transport–corrected scattering length for the 2% medium at 720 nm was estimated at 0.3–0.5 mm. One rod was inserted into the cylinder as a heterogeneity, halfway between the center and boundary. The sources were normally incident at 6 different locations around the phantom and the detectors were located at 20 different locations (10° separation in angle) for each source (Figure 2C). Escaping photons were collected using a Hamamatsu CCD camera and the readings were normalized according to the lens aperture, exposure time, camera gain, and intensity of the laser source. The

differences between the reference and target media readings were then calculated for image reconstruction.

To study the effect of random error, different levels of Gaussian white noise — 1%, 5%, 10%, 50%, 100%, and 500%, where the noise level is defined as 100 times the ratio of noise variance to average signal power — were generated using a random number generator [10]. The generated noise was then added to the detector readings, the weight matrix, or both. The detector readings and weight matrices were then used for image reconstruction, using a constrained CGD method [11], and the reconstructed images were compared. As a control, reconstructions were also performed using only generated Gaussian white noise as the detector readings, and the noise–free matched weight matrix.

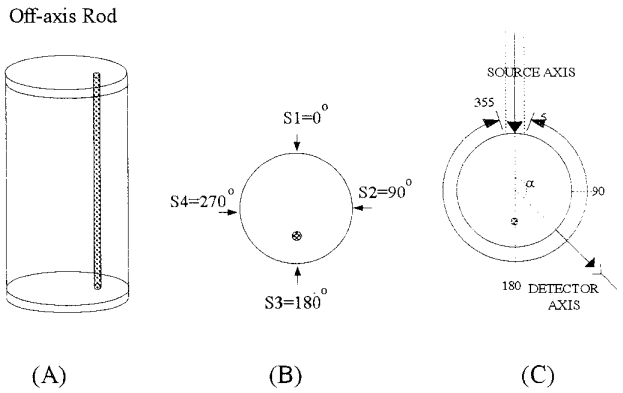

Figure 1. (A) Tissue phantom used for Monte Carlo simulations. (B) Source configuration. (C) Simulation detector configuration for each source. The detectors were located every 10° about the boundary of the phantom

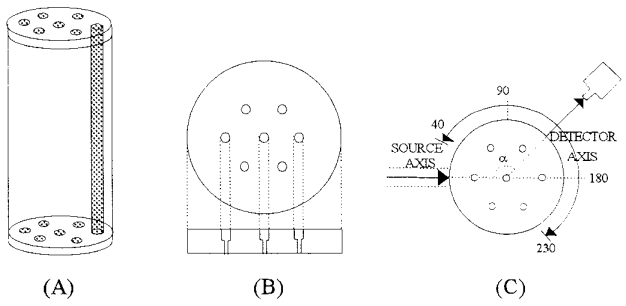

Figure 2. Tissue phantom used for experiments: (A) side view, (B) top view, and (C) experimental source and detector configuration.

IV. Results

Figure 3 shows the reconstructed images from MCS–generated data using the constrained CGD method after 1,000 iterations. Figure 3A is the target image and Figure 3B is the reconstructed image using the matched weight matrix. Figures 3C–E demonstrate the reconstructed images using unmatched weight matrices for media of 10, 40, and 100 mfp diameter, respectively. Figure 4 shows the reconstruction results for experimental data.

Figure 5 shows the images reconstructed from simulation data with 5%, 10%, 100%, and 500 % white noise added to the detector readings. Figure 6 illustrates the reconstruction results for the 10% added noise case after 10, 100, and 1,000 iterations. Figure 7 demonstrates the results for the noise–free detector readings with 1%, 5%, and 10% white noise added to the matched weight matrix, and Figure 8 shows the reconstructed images for the 5% noise case after 10, 100, and 1,000 iterations. Figure 9 illustrates reconstruction results from the simulation data with 1%, 5%, and 10% added white noise in both the detector readings and weight matrices. Figure 10 shows the results from the pure noise data after 100 iterations, where the indicated 1%, 10%, and 100% noise levels are the same as those added to the detector readings.

V. Discussion And Conclusions

Currently applicable image reconstruction schemes in optical tomography require *a priori* knowledge of the physical properties of the reference or background medium, which is generally difficult to obtain. The use of other image modalities, *e.g.*, CT or MR, provides a convenient way to estimate the physical properties but introduces a mismatch in the weight matrices. Our analysis of a simply structured phantom shows that good quality (*i.e.*, few artifacts, size and shape of image peak nearly correct, sharp edge detection) images (Figure 3B) can be obtained, and the rod can be accurately located, when the reconstruction is based on noiseless detector readings and the matched weight matrix. Good image quality was also obtained for unmatched weight matrices (Figure 3C, 3D, 3E), but the location of the rod in the image becomes increasingly inaccurate as the mismatch increases. Examination of the experimental data results reveals a similar trend. Images with a clear rod–like structure and some artifacts were obtained in all four reconstructions (Figures 4B–E) while the locations of the rods move from the border to the center of the cylinder as the diameter (in units of mfp) of the cylinder increases.

The noise study shows that the reconstruction algorithm is much more sensitive to noise in the weight matrix than to noise in the detector readings. The location of the rod can be identified with reasonable accuracy with as much as 100% noise (noise variance over power of detector readings is 1.0; Figures 5A, 5B, 5C) added to the detector reading, but 5% (Figures 7A, 7B, 7C) noise added to the weight matrix is sufficient to produce an image consisting of nothing but artifacts. When the same amount of noise was added to both detector readings and weight matrix, the noise added to the weight matrix has the more dominant effect on the reconstruction results (compare Figures 5, 7, and 9). The impact of noise on an image increases with the number of iterations of the reconstruction algorithm when noise is

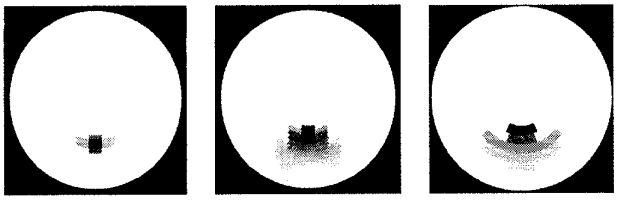

(A) Target (B) 20 mfp (C) 10 mfp

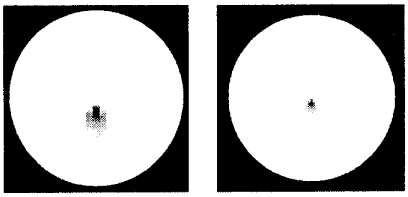

(D) 40 mfp (E) 100 mfp

Figure 3. Reconstructed images from simulation data using CGD method after 1,000 iterations, with matched weight matrix (B), and unmatched matrices (C), (D), and (E). (A) is the target image.

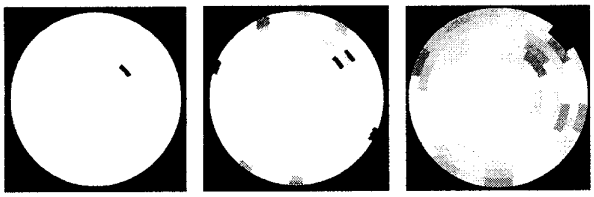

(A) Target (B) 20 mfp (C) 10 mfp

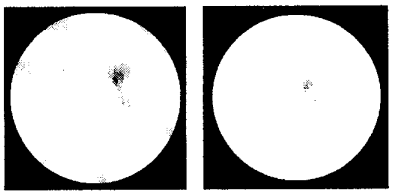

(D) 40 mfp (E) 100 mfp

Figure 4. Reconstructed images from experimental data using CGD method after 1,000 iterations, with matched weight matrix (B), and unmatched matrices (C), (D), and (E). (A) is the target image.

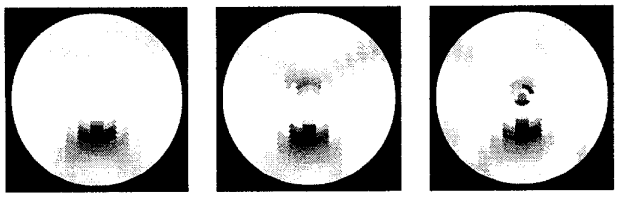

(A) 5% (B) 10% (C) 100%

(D) 500%

Figure 5. Images reconstructed from simulation detector readings after 100 iterations, with noise added to the detector readings: (A) 5%, (B) 10%, (C) 100%, and (D) 500 %. The target is the same as shown in Figure 3A.

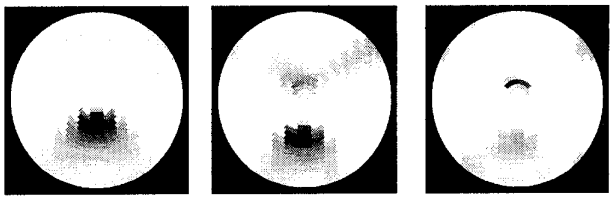

(A) 10 iterations (B) 100 iterations (C) 1,000 iterations

Figure 6. Reconstructed images from simulation data with 10% added noise to detector readings after (A) 10 iterations, (B) 100 iterations, and (C) 1,000 iterations. The target is the same as shown in Figure 3A.

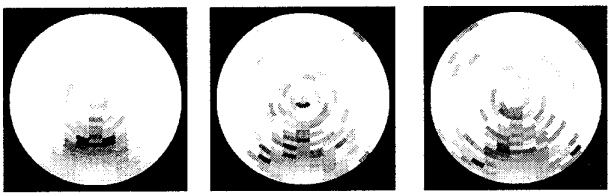

(A) 1% (B) 5% (C) 10%

Figure 7. Reconstructed images from simulation data with noise added to the weight matrix: (A) 1%, (B) 5%, (C) 10%, after 100 iterations. The target is the same as shown in Figure 3A.

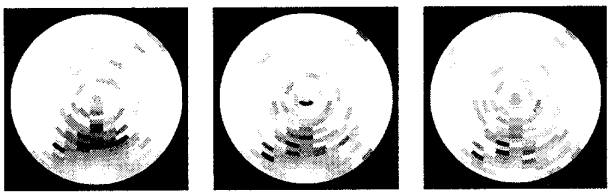

(A) 10 iterations (B) 100 iterations (C) 1,000 iterations

Figure 8. Reconstructed images from simulation data with 5% added noise after (A) 10 iterations, (B) 100 iterations, and (C) 1,000 iterations. The target is the same as shown in Figure 3A.

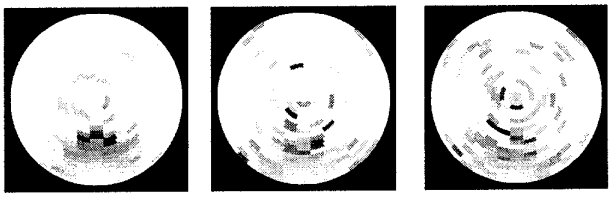

(A) 1% (B) 5% (C) 10%

Figure 9. Reconstructed images from simulation data with added noise in both the detector readings and the weight matrix: (A) 1%, (B) 5%, (C) 10%, after 100 iterations. The target image is the same as shown in Figure 3A.

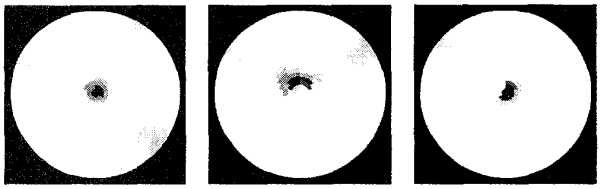

(A) 1% (B) 10% (C) 100%

Figure 10. Reconstructed images from pure noise data to the detector readings: (A) 1%, (B) 10%, (C) 100%, after 100 iterations.

added to the detector readings (Figures 6). There is not such a clear trend, however, when noise is added to the weight matrix (Figure 8).

There is a plausible, testable explanation for these phenomena. When noise is added to the detector readings, we can conveniently consider the reconstructed image as a sum of a noiseless detector readings image and a pure noise image (this is not strictly true, because positivity constraints were imposed on the reconstruction results, and this makes the inverse problem nonlinear). Because noise is randomly added to the detector readings, it is evenly distributed in all directions in the detector readings space. Because the CGD algorithm updates voxels by moving the evolving solution in the direction of the conjugate gradient, those voxels with the highest weights will "respond" to noise in earlier iterations due to their greater contributions to the gradient. Thus, the spatial extent of the noise effect seen in early stages of the reconstruction is quite limited, and the magnitude of the effect is much smaller than that of the noiseless detector readings (Figure 6A). As the number of iterations increases, the noise effect spreads out over the entire volume involved in the reconstruction and finally dominates the results (Figure 6C). On the other hand, when noise is added to the weight matrix, it causes a structural change in the imaging operator. Thus, we can treat the addition of noise as the introduction of random mismatches into the weight matrix. In comparison to the results from systematically mismatched weight matrix in Figures 3 and 4, the randomly mismatched weight matrices causes more structural change than position change in the reconstructed images (Figure 8).

The "images" obtained when pure noise (Figure 10) was substituted for **R** have a randomized structure, with the greatest image intensity in voxels near the cylinder axis. This is consistent with the ill–conditioned structure of the weight matrix, whose columns representing voxels near the axis contain much smaller elements than those in columns corresponding to peripheral voxels.

This study demonstrates the effect of mismatched weight matrices and noise on the image reconstruction in optical diffusion tomography. Ongoing research includes further study of the quality of images reconstructed from noise–corrupted data, using different source–detector configurations, and incorporating regularization [12] and total least squares [13] techniques to enhance image quality.

VI. Acknowledgment

This work was supported in part by NIH grant R01 CA59955, by ONR grant No. 00149510063, and by the New York State Science and Technology Foundation.

VII. References

1. *Proc. Optical Tomography, Photon Migration, and Spectroscopy of Tissue and Model Media: Theory, Human Studies, and Instrumentation*, B. Chance and R. R. Alfano, eds., vol. SPIE–2389, (San Jose), Feb. 1995.
2. *Medical Optical Tomography: Functional Imaging and Monitoring*, G. Müller *et al.*, eds., SPIE Institutes vol. IS11, SPIE Press, Bellingham, WA, 1993.
3. J. Chang, R. L. Barbour, H. Graber, and R. Aronson, "Fluorescence optical tomography," vol. SPIE–2570, (San Diego), 1995, in press
4. J. Chang, R. Aronson, H. L. Graber, R. L. Barbour "Imaging diffusive media using time–independent and time–harmonic sources: dependence of image quality on imaging algorithms, target volume, weight matrix, and view angles," vol. SPIE–2389, pp. 448–464, (San Jose), Feb. 1995.
5. S. R. Arridge and M. Schweiger, "Sensitivity to prior knowledge in optical tomographic reconstruction," vol. SPIE–2389, pp. 378–388, Feb. 1995.
6. W. C. Chew and Y. M. Wang, "Reconstruction of two–dimensional permittivity distribution using the distorted Born iterative method," *IEEE Trans. Med. Imag.*, vol. 9, pp. 218–225, 1990.
7. J. Chang, H. L. Graber, R. L. Barbour, "Progress toward optical mammography: imaging in dense scattering media using time–independent optical sources," in *Proc. of 1994 IEEE Medical Imaging Conference*, pp. 1484–1488, (Norfolk, VA), Nov. 1994.
8. J. Chang, Y. Wang, R. Aronson, H. L. Graber, and R. L. Barbour, "A Layer Stripping Approach for Recovery of Scattering Medium Using Time–Resolved Data," vol. SPIE–1767, (San Diego), July 1992.
9. S. R. Arridge, M. Schweiger, D. T. Delpy., "Iterative reconstruction of near infrared absorption images," *ibid.*, pp. 372–383.
10. W. H. Preuss *et al.*, *Numerical Recipes in FORTRAN*, 2nd ed., Cambridge U. Press, 1992.
11. J. Chang, H. L. Graber, and R. L. Barbour, "Image reconstruction of dense scattering media from CW sources using constrained CGD and a matrix rescaling technique," vol. SPIE–2389, pp. 448–464, (San Jose), Feb. 1995.
12. W. Zhu, Y. Wang, H. L. Graber, R. L., Barbour, and J. Chang, J. "A regularized progressive expansion algorithm for recovery of scattering media from time–resolved data," *OSA Proceedings on Advances in Optical Imaging and Photon Migration*, vol. 21, pp. 211–216, (Orlando), Mar. 1994.
13. W. Z. Zhu, Y. Wang, J. Chang, H. L. Graber, and R. L. Barbour, "Image reconstruction in scattering media from time–independent data: a total least squares approach," vol. SPIE–2389, pp. 420–430, (San Jose), Feb. 1995.